Curie Transition and Piezoelectricity of the Blends of a Ferroelectric VDF/TrFE Copolymer and PMMA

KAP JIN KIM* and GWAN BUM KIM

Department of Textile Engineering, College of Engineering, Kyung Hee University, #1 Seochun-ri, Kiheung-eup, Yongin-kun, Kyunggi-do 449-701, South Korea

SYNOPSIS

The Curie transition, even though the conformational change at the Curie transition primarily arises from intermolecular interaction, is highly dependent on the crystallization conditions. A slower cooling rate from the melt during paraelectric crystallization lowers T_c, increases the portion of F_β at the expense of F_α reduction, and produces a more unstable ferroelectric phase. $T_c^\downarrow$ is rarely dependent upon the amount of PMMA, but $T_c^\uparrow$ is increased with the PMMA content. PMMA has a favorable action in forming a more stable ferroelectric phase in the P(VDF/TrFE)/PMMA blend and elevating the Curie transition point because of the all-*trans* sequence conformation of PMMA and a specific intermolecular interaction with P(VDF/TrFE) in the melt state. However, PMMA reduces the total amount of the crystalline phase, the electric response, and the piezoelectricity. © 1993 John Wiley & Sons, Inc.

INTRODUCTION

The random copolymers of vinylidene fluoride (VDF) and trifluoroethylene (TrFE) having piezoelectric and pyroelectric properties normally have a Curie transition at which ferroelectricity is lost through a solid-state order–disorder phase transition and they become paraelectric.[1,2] This Curie transition accompanies many changes in chain conformation, crystal structure, enthalpy, dielectricity, etc., which are identified by IR spectroscopy,[3-5] X-ray diffraction,[6-8] DSC,[9-11] and other electric measuring devices.[9,10,12] The Curie transition behavior is affected by many factors. The content of VDF in the copolymer affects the Curie transition more significantly than do any other factors. Transition temperature is increased with the content of VDF.[2,9] Hydrostatic[13-15] and tensile[16] stresses affect more or less the Curie transition behavior. The transition behavior is also influenced remarkably by the sample preparation conditions such as thermal and solution history.[4,11,17] The increase of crystallinity and the reduction of conformational defects of crystallites by the poling process affect the Curie transition behavior.[18,19] Even though there have been many reports on the Curie transition behavior of the VDF copolymer as reviewed above, few reports refer to the phase transition behavior of the blend of the VDF copolymer and a compatible amorphous polymer and the effect of systematic crystallization on the phase transition of the blend. In this paper, as the second successive study on the P(VDF/TrFE)/PMMA blend, we focus our attention on the effects of melt-crystallization condition, poling, and content of a compatible amorphous PMMA on the ferroelectric phase transition, infrared spectra, crystalline structure, and piezoelectricity of the P(VDF/TrFE)/PMMA blend system.

EXPERIMENTAL

Films of P(VDF/TrFE) having a molar ratio of 75/25, *a*-PMMA, and their mixtures were cast from 2 or 5% acetone solution onto glass plates, quickly transferred to the drying oven maintained at 50°C, dried for 1 h, and further dried under vacuum for 24 h. Thermal analysis was performed using a Perkin-Elmer DSC-4. After samples were kept at 180°C

* To whom correspondence should be addressed.

Journal of Applied Polymer Science, Vol. 47, 1781–1789 (1993)
 CCC 0021-8995/93/101781-09

for 10 min on the DSC, molten samples were cooled to 80°C at various cooling rates to obtain samples differing in thermal history and then cooled to 20°C at 10°C/min regardless of the previous rate of cooling used for melt crystallization in order to obtain the exothermic peak of the paraelectric-to-ferroelectric phase transition. Upon heating again to 160°C at 10°C/min, two endothermic peaks for the Curie transition and melting were recorded. These transition peaks were analyzed to observe the effect of thermal history on the transition temperature and the enthalpic change in transition caused by differences in the rates of cooling through the initial paraelectric phase crystallization temperature range.

To investigate the electric response of the sample after poling, the IR spectrum of the sample (cast from 2% solution and thickness of about 10 μm) annealed at 130°C for 24 h was recorded first and then the poled IR spectrum was obtained with the same sample after it was sandwiched between aluminum electrodes and subsequently poled under the electric strength of 0.7 MV/cm at room temperature for about 10 min. IR measurements were made on Perkin-Elmer FTIR 1760X with the resolution of 2 cm^{-1} and 32 scans.

The film (thickness 50–80 μm) cast from 5% solution and subsequently annealed at 130°C for 24 h was used for X-ray and piezoelectic constant measurement. Prior to the measurement of piezoelectricity, the film was poled at 80°C under the electric strength of 0.7 MV/cm for 30 min in silicon oil to prevent electrical breakdown. The piezoelectric stress constant was measured using a Rheovibron charge amplifier RHEO-20 with 110 Hz in the range of 30–40°C. X-ray measurement was carried out with Rigaku X-ray diffractometer RAD-IIA.

RESULTS AND DISCUSSION

To observe the effect of cooling rate used for the nonisothermal melt crystallization on the exothermic paraelectric-to-ferroelectric ($P \Rightarrow F$) phase transition, molten samples were cooled to 80°C at six different cooling rates, i.e., 2, 4, 8, 16, 30, and 60°C/min and further cooled to room temperature at 10°C/min to observe the phase transition. A fixed cooling rate of 10°C/min was used to prevent the transition curve from shifting by different supercooling due to the different cooling rates in the $P \Rightarrow F$ transition range. Figure 1(a) shows the exothermic curves for the $P \Rightarrow F$ transition for P(VDF/TrFE) crystallized nonisothermally at different rates of cooling. Each curve is composed of three peaks, which are designated as α, β, and γ in descending temperature order. Figure 1(b) shows the endothermic curves for the ferroelectric-to-paraelectric ($F \Rightarrow P$) phase transition obtained by the subsequent heating to 160°C at 10°C/min. In this case, the peaks are not distinctly separated, but show only the α peak and the β peak as a shoulder. The γ peak is buried in the broad β peak. This multiple transition behavior was also reported by Davis et al.[7] and Tanaka et al.[17] for P(VDF/TrFE) with more than 65 mol % VDF. Davis et al. only reported the result without further discussion about the origin

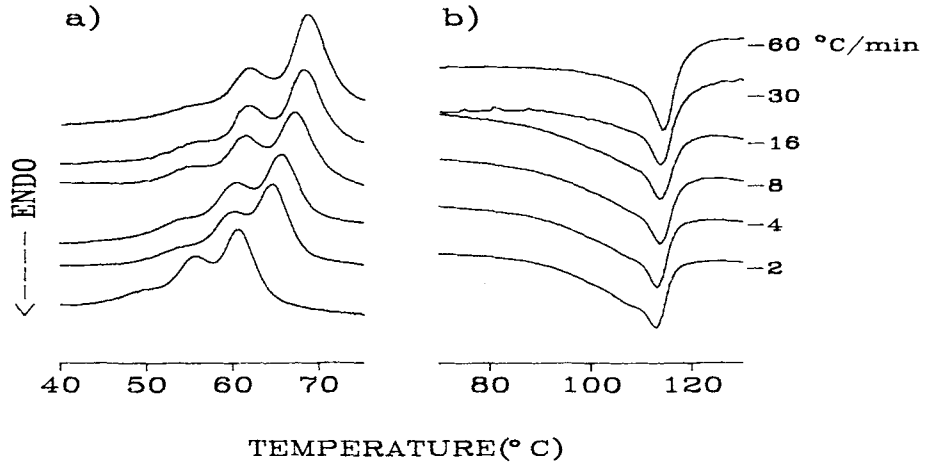

Figure 1 DSC thermograms for (a) the $P \Rightarrow F$ phase transition and (b) the $F \Rightarrow P$ phase transition of P(VDF/TrFE) crystallized nonisothermally at various rates of cooling from the melt to 80°C. (a) Cooling rate from 80 to 30°C is 10°C/min; (b) heating rate from 30 to 160°C is 10°C/min.

of multiple Curie transition. Tanaka et al. discussed multiple transition in more detail, which will be discussed later. Koga and Ohigashi[19] also reported that multiple peaks around the Curie transition temperature are associated with the ferroelectric β phase including conformational defects composed of some *gauche* isomers, i.e., these peaks may correspond to the transition from the paraelectric phase to the all-*trans* β phase, γ phase (T_3GT_3G'), and α phase (TGTG') on cooling. But their analysis has not been proved clearly yet.

As shown in Figure 1(a), the peak temperature corresponding to the $P \Rightarrow F$ transition (denoted by $T_c^{\downarrow}$) in the cooling process after nonisothermal crystallization are shifted to higher temperatures with increasing rates of cooling through the paraelectric crystallization region. The α peak temperature ($T_{c,\alpha}^{\downarrow}$) is shifted much more than are the β and γ peaks ($T_{c,\beta}^{\downarrow}$ and $T_{c,\gamma}^{\downarrow}$). Also, in Figure 1(b), peak temperatures corresponding to the $F \Rightarrow P$ transition (denoted by $T_c^{\uparrow}$) in the heating process are shifted to the right as the cooling rate through the paraelectric crystallization region is increased, but the magnitude of the shift is much less than in the cooling process. Changing the cooling rate from 2 to 60°C/min causes changes of over 5°C and 2°C in the $T_{c,\alpha}^{\downarrow}$ and $T_{c,\alpha}^{\uparrow}$, respectively. Since the Curie transition is a first-order transition,[12] it necessarily shows a large thermal hysteresis upon cooling and heating. Here, the magnitude of hysteresis dependent on the cooling rate is estimated by the difference between $T_{c,\alpha}^{\uparrow}$ and $T_{c,\alpha}^{\downarrow}$. As the cooling rate is increased, the thermal hysteresis becomes smaller.

The reason the Curie transition temperature is highly dependent on the crystallization cooling rate can be explained as follows: As the Curie transition is an order–disorder or disorder–order transition in the crystalline phase, the crystallization conditions such as the cooling rate and the crystallization temperature affecting the crystalline structures such as packing density, lamellar thickness, crystalline defect, crystallinity, etc., should have a direct effect on the ferroelectric phase transition. The effect of the cooling rate on the Curie transition can be generally explained, based on the thermodynamic point of view in Figure 2, illustrating the chemical potential vs. temperature for the ferroelectric, paraelectric, and melt phases, where μ_F, μ_P, and μ_M stand for the chemical potential of each phase. The Curie transition temperature is considered as an intersecting point of the μ_F and μ_P lines. Similarly, the melting point is an intersection of the μ_P and μ_M lines. The downward shift of the μ_P line, i.e., the formation of more stabilized paraelectric crystalline phase and/

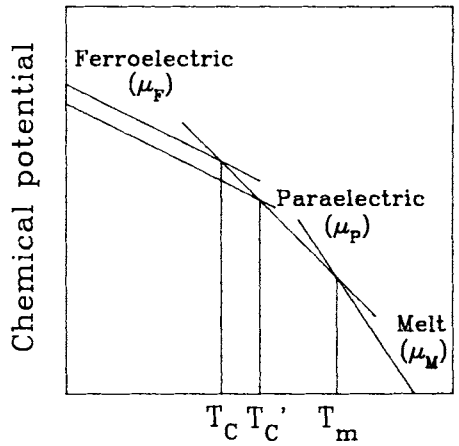

Figure 2 Chemical potential of the ferroelectric, paraelectric, and melt phases of P(VDF/TrFE) as a function of temperature.

or the upward shift of the μ_F line, i.e., the formation of less stabilized ferroelectric crystalline phase cause the depression of the Curie transition temperature. The downward shift of the μ_P line also results in the elevation of the melting point, but the only upward shift of the μ_F line cannot change the melting point at all.

Since nonisothermal crystallization occurs only in the paraelectric phase region in this experiment, the thermodynamic properties of the formed paraelectric crystallites are highly dependent on the cooling rate from the melt phase to 80°C. Slower cooling would enable the paraelectric crystal phase to have more time required for the growth and the better reorganization of the crystal. Thus, the paraelectric phases crystallized during slower cooling would have better organization and fewer defects than those crystallized during a more rapid cooling. As a result, the depression of T_c is thought to become greater with a decrease in the cooling rate due to the downward shift of the μ_P line. Further cooling to room temperature transforms the paraelectric crystal into the ferroelectric crystal accompanying a conformational change from the *gauche* state to the *trans* state. The crystalline structure of the ferroelectric phase formed upon further cooling from 80°C to room temperature is not independent of the crystalline structure of the corresponding paraelectric crystal phase before subsequent cooling, but highly dependent on the thermodynamic stability of the previous paraelectric crystal phase. In a more stable paraelectric crystal formed with slower cooling, the paraelectric crystal phase shows lower T_c resulting from the upward shift of the μ_F line due to the difficulty in transformation to a complete fer-

roelectric phase and from the downward shift of the μ_P line due to the formation of a more stable paraelectric crystal phase.

Triple peaks and double peaks in the phase transition region observed on the DSC, when cooled and heated, respectively, seem to reflect the ferroelectric transition of two and/or three different crystalline structures. Tanaka et al.[17] reported that double peaks were observed in the phase transition region when the copolymer containing 65 mol % VDF crystallized above its T_c was heated from room temperature to the melting temperature. They explained the higher temperature peak corresponds to the $F \Rightarrow P$ transition of more ordered ferroelectric crystals and the lower temperature peak to that of less ordered ferroelectrets. In a VDF/TrFE(52/58) copolymer, only the lower transition temperature peak was observed regardless of the crystallization temperature. In a VDF/TrFE(73/27) copolymer, a lower transition temperature peak was detected only when it is crystallized at 140°C. In most cases, it showed only the higher transition temperature peak. In our experiment, the three distinct exothermic peaks, observed in all the P(VDF/TrFE) samples upon further cooling at the rate of 10°C/min after nonisothermal crystallization at the various rates of cooling, seem to correspond to the transition of paraelectric crystals to three different types of ferroelectric crystalline structures. However, these three different ferroelectric crystals have not been identified by any other methods. Infrared spectroscopy could not identify any difference between them because they may have the same chain conformation despite of different crystalline structure. A more sophisticated X-ray study is expected to reveal the crystalline structures of the three kinds of ferroelectric phases.

As mentioned earlier, we define again the crystalline structure having the highest transition temperature (T_α) as the ferroelectric α phase (F_α), that having the medium transition temperature (T_β) as the F_β phase, and that having the lowest one (T_γ) as the F_γ phase. Figure 1(a) shows a clear tendency that $T_{c,\alpha}^{\downarrow}$ is shifted much more to the lower temperature than are the other transition temperatures and the peak height at $T_{c,\alpha}^{\downarrow}$ decreases and the other two peak heights increase with a decrease in the rate of cooling for nonisothermal crystallization. This result indicates that the F_α phase has a highly ordered ferroelectric crystalline structure. On the other hand, the F_β and F_γ phases are less ordered ferroelectric crystals. Since the stable paraelectric crystal phase cannot be transformed easily to the highly ordered ferroelectric phase upon cooling as discussed earlier, slower cooling, inducing crystallization into the more stable paraelectric phase, results in an increase in the amount the F_β and F_γ phases having less ordered ferroelectric crystalline structure at the expense of the F_α phase content. Changes in the cooling rate used for nonisothermal crystallization have a greater effect on the perfection and/or packing for the F_α phase than for the F_β and F_γ phases.

As in the case of the $P \Rightarrow F$ phase transition observed upon cooling, we could observe two $F \Rightarrow P$ transitions for the slowly cooled samples upon subsequent heating in Figure 1(b). The higher transition temperature peak corresponds to the transition of the F_α phase to the paraelectric crystal phase and the lower transition temperature peak to that of the F_β phase to the paraelectric phase. The transition peak for $F_\gamma \Rightarrow P$ could not be discerned, but the endotherm was broader the slower the rate of cooling for crystallization. The trend in the shift of peak temperature and change in peak height with the cooling rate is the same as in the case of the $P \Rightarrow F$ transition, but changes in $T_{c,\alpha}^{\uparrow}$ and $T_{c,\beta}^{\uparrow}$ are much smaller than those in $T_{c,\alpha}^{\downarrow}$, $T_{c,\beta}^{\downarrow}$, and $T_{c,\gamma}^{\downarrow}$ and are dependent on the cooling rate. Because the ferroelectric phases formed initially are reorganized structurally to a more stable ferroelectric phase or the ferroelectric phase is formed newly from the amorphous phase during heating on the DSC, no big difference between samples crystallized at different cooling rates was discernible. Thus, the heat of the $P \Rightarrow F$ transition is decreased with increasing cooling rates, but that of the $F \Rightarrow P$ transition is nearly constant regardless of the rate of cooling.

Figure 3(a) shows the exothermic curves for the $P \Rightarrow F$ transition for a P(VDF/TrFE)/PMMA (85/15) blend crystallized nonisothermally. Even though the trend of peak shift with the rate of cooling for crystallization is equal to that of P(VDF/TrFE), there are triple transition peaks only for the very slow cooling rate and the $T_{c,\beta}^{\downarrow}$ and $T_{c,\gamma}^{\downarrow}$ peaks are not clear or disappear at the higher cooling rates. There are no big differences in $T_{c,\alpha}^{\downarrow}$ between P(VDF/TrFE) and its blends, but $T_{c,\beta}^{\downarrow}$ of the blend is lower than that of P(VDF/TrFE) at the same cooling rate for the melt crystallization. Since PMMA reduces significantly the rate of crystallization when cooled from melt as discussed in the previous paper,[20] the paraelectric crystal formed in the blend is less stable than in the P(VDF/TrFE) and, consequently, the content of F_α phase of the blend is relatively higher than those of F_β and F_γ when compared with the P(VDF/TrFE). The fact that the $T_{c,\beta}^{\downarrow}$ of the blend is lower than that of P(VDF/TrFE) indicates that there must be more defects in

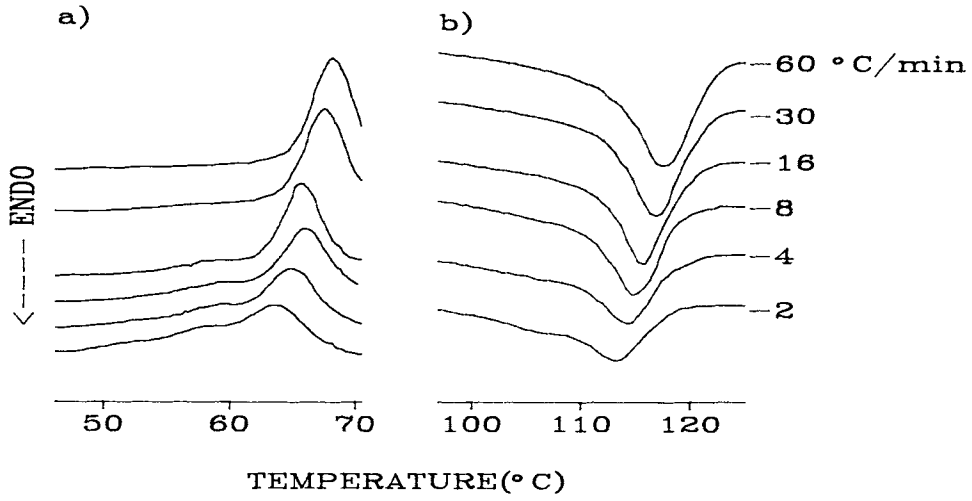

Figure 3 DSC thermograms for (a) the $P \Rightarrow F$ phase transition and (b) the $F \Rightarrow P$ phase transition of the P(VDF/TrFE)/PMMA(85/15) blend crystallized nonisothermally at various rates of cooling from the melt to 80°C. (a) Cooling rate from 80 to 30°C is 10°C/min; (b) heating rate from 30 to 160°C is 10°C/min.

the F_β phase of the blend than in the copolymer alone. Figure 3(b) shows the endothermic curves for the $F \Rightarrow P$ phase transition obtained by subsequent heating. There are no differences in the overall trends of peak shift and curve shapes as a function of cooling rate between the blend and copolymer alone.

The thermal characteristics of the P(VDF/TrFE)/PMMA blends crystallized from the melt at 10°C/min are summarized in Table I. The decrease of the $T_{c,\beta}^{\downarrow}$ of the blends may be attributed to the increase in defects in the F_β phase with an increase in the content of PMMA. Although $T_{c,\alpha}^{\downarrow}$ is nearly constant, $T_{c,\alpha}^{\uparrow}$ increases with an increase of the content of PMMA. From this result, it is considered that PMMA has a favorable action in the reorganization of the initially formed ferroelectric crystal phase into conformationally less defective phase and more highly packed crystal during heating on the DSC. Since PMMA has a nearly all-*trans* sequence conformation in the melt of the blend[21] and a specific intermolecular interaction with P(VDF/TrFE) exists as revealed in the previous paper,[20] the paraelectric phase with a long-*trans* sequence defect is relatively easily formed and, subsequently, the more stable ferroelectric phase with less *gauche* isomers can be obtained after the $P \Rightarrow F$ transition. Thus, the ferroelectric phase formed initially through the $P \Rightarrow F$ transition can easily be reorganized into the more stable phase with a smaller *gauche* defect during heating on the DSC, which results in the increase of $T_{c,\alpha}^{\uparrow}$ with an increase in PMMA content. This result is contradictory to Saito et al.'s report[22] that the addition of PMMA did not affect the Curie point since the conformational change at T_c primarily arises from intramolecular interaction, whereas the melting behavior involves both intra- and intermolecular interactions. The decrease in the heat of the Curie transition is considered to result from the reduction of the amount of paraelectric crystal formed due to the prohibiting action of PMMA in crystallization. The magnitude of $\Delta H_c^{\uparrow}$ is always larger than that of $\Delta H_c^{\downarrow}$ regardless of the content of PMMA. From this, a small amount of a new ferroelectric phase is expected to be formed during rescanning on the DSC, from the amorphous phase or the paraelectric phase still remaining even after the $P \Rightarrow F$ transition. As

Table I Curie Transition Behavior of the P(VDF/TrFE)/PMMA Blends Crystallized from the Melt at the Rate of −10°C/Min

PMMA (wt %)	$T_{c,\alpha}^{\downarrow}$ (°C)	$T_{c,\beta}^{\downarrow}$ (°C)	$T_{c,\alpha}^{\uparrow}$ (°C)	$\Delta H_c^{\downarrow}$ [cal/g of P(VDF/TrFE)]	$\Delta H_c^{\uparrow}$ [cal/g of P(VDF/TrFE)]
0	66.3	60.3	113.7	4.63	5.94
5	66.5	60.4	113.8	4.42	5.95
10	66.6	59.7	114.2	4.04	5.39
15	66.2	58.7	115.0	3.86	4.99
20	67.0	58.0	116.1	3.58	4.44
25	66.2	57.8	115.0	2.15	2.70

the melting behavior of the P(VDF/TrFE)/PMMA system was throughly discussed in the previous papers,[20,22] no further mention will be made here.

The dependence of $T^{\uparrow}_{c,\alpha}$ on the PMMA content at various rates of cooling is shown in Figure 4. For the rates of cooling from the melt greater than 4°C/min, $T^{\uparrow}_{c,\alpha}$ increases with the PMMA content up to 20 wt % and then declines above that content. This result is attributed to the favorable action of PMMA in forming the more stable ferroelectric phase with less *gauche* content, as discussed above. The decrease of $T^{\uparrow}_{c,\alpha}$ above 20 wt % PMMA arises from increasing morphological defects due to rapid reduction of the crystallization rates. We, however, still cannot give a clear explanation why $T^{\uparrow}_{c,\alpha}$ shows a gradual decrease as a function of the PMMA content at the very slow cooling rate: 2°C/min.

The irreversible rotation of CF dipole by poling and the changes in chain conformation and crystalline packing density arising from the dipole rotation are identified by the changes in the IR spectrum,[23] DSC,[24] X-ray diffraction pattern, etc.[25] This irreversible dipole rotation is one of the main causes of the piezo- and pyroelectricities of VDF/TrFE copolymers. Figure 5 shows the changes in the P(VDF/TrFE) IR spectra in the CH stretching region after poling. Since the two peaks, assigned to asymmetric (3012 cm^{-1}) and symmetric stretching (2987 cm^{-1}) vibrations of CH, are of isolated vibration mode, they are insensitive to conformational change during poling, whereas they are very sensitive to the rotation of CH groups. As in this experiment

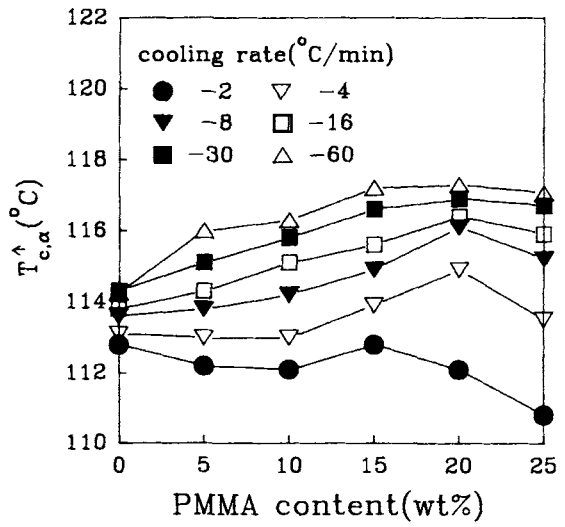

Figure 4 Dependence of $T^{\uparrow}_{c,\alpha}$ on the PMMA content for the specimens crystallized nonisothermally at various rates of cooling.

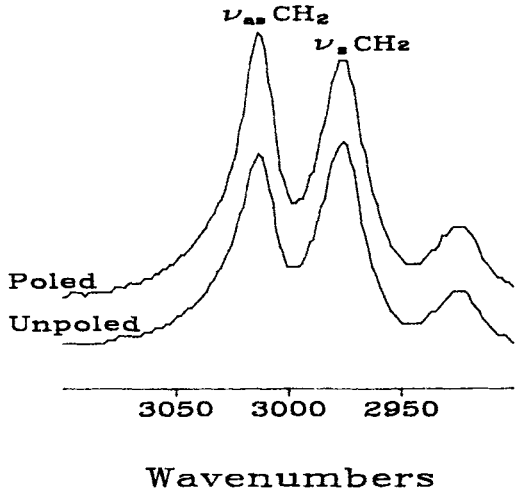

Figure 5 Changes in the absorbance IR spectra of the P(VDF/TrFE) film as a function of poling in the region 3100–2900 cm^{-1}.

the CF dipole is aligned to the electric field direction during poling and the propagation direction of the IR beam is parallel to the applied electric field, the absorbance of $\nu_s CH_2$ is naturally reduced, but that of $\nu_{as} CH_2$ is increased. The clear change in absorbance of IR is observed after poling in Figure 5, which is a good example of the irrevisible dipole rotation after poling. The degree of orientation of the CH or CF dipole along the external electric field, which is calculated from the relative change in IR absorbance, is expected to have a strong relationship with the piezoelectricity. The calculation of the degree of orientation of the CH or CF dipole was reported in the previous paper.[26] However, it is impossible to estimate the CF dipole orientation in the P(VDF/TrFE)/PMMA blend system, as the absorbance peaks of CH stretching for PMMA are superimposed. Therefore, other absorbance bands must be found to estimate the dipole orientation in the blend.

IR spectra (1500–700 cm^{-1} region) obtained for the annealed and poled P(VDF/TrFE) films are shown in Figure 6(a). As predicted above, localized specific vibrations associated with the CF dipole exhibit the largest intensity changes. The changes in intensities at 1290 ($\nu_s CF_2 + \nu_s CC + \delta_s CCC$, long *trans* sequence), 884 ($\rho CH_2 + \nu_a CF_2 + \rho CF_2$, *trans*), and 848 ($\nu_s CF_2 + \nu_s CC$, long *trans* sequence) cm^{-1} as a function of poling are attributed to the alignment of CF dipoles in the electric field direction and the increase or decrease in the long *trans* sequences through field-induced structural reorganization. Nevertheless, the significant changes in intensity at

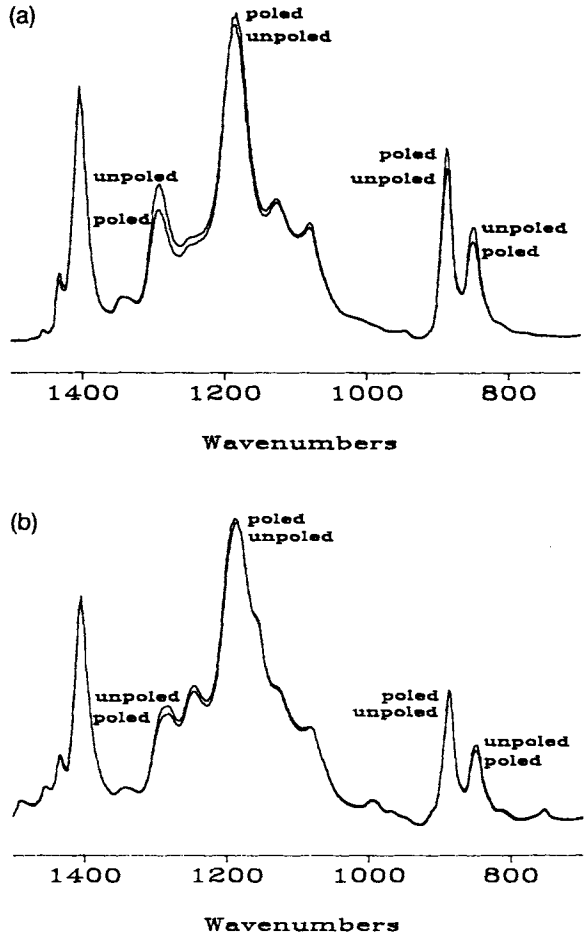

Figure 6 (a) Changes in the absorbance IR spectra of the P(VDF/TrFE) film as a function of poling in the region 1500–700 cm^{-1}. (b) Changes in the absorbance IR spectra of the P(VDF/TrFE)/PMMA (80/20) film as a function of poling in the region 1500–700 cm^{-1}.

these three bands indicate the extensive electric response such as the CF dipole alignment toward the electric field direction during the poling procedure. Figure 6(b) shows the IR spectra for the 80/20 blend before and after poling. The changes in IR intensities as a function of poling are relatively small compared with the case of a P(VDF/TrFE) sample. It has been shown in the previous paper that, with the CF dipole aligned to the electric field direction, the intensity of 884 cm^{-1} peak is increased and those of 1290 and 848 cm^{-1} peaks are reduced.[23,26] Additionally, because the 884 and 848 peaks do not overlap with the characteristic peaks of PMMA, the percentage of change in the ratio of intensity at 884 cm^{-1} to intensity at 848 cm^{-1} (A_{884}/A_{848}) by poling can be used to estimate the degree of the electric response of the CF dipole as a function of the PMMA content. As shown in Figure 7, the relative change

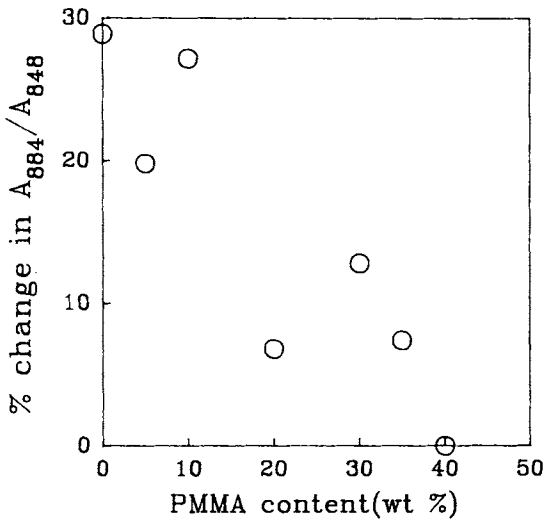

Figure 7 Changes in the ratio of A_{884}/A_{848} after poling as a function of the PMMA content.

is drastically reduced with an increase in the PMMA portion, and no changes are observed after the PMMA content exceeds 40%. This may result from the great reduction of crystallinity with an increase in the PMMA content, as shown in the above discussion and X-ray diffraction in Figure 8.

Since the structural reorganization through poling can produce more stable ferroelectric phase having a small amount of *gauche* defects and high packing density as discussed in the previous paper,[26] the Curie point is expected to move to the higher temperatures and the height of the diffraction peak cor-

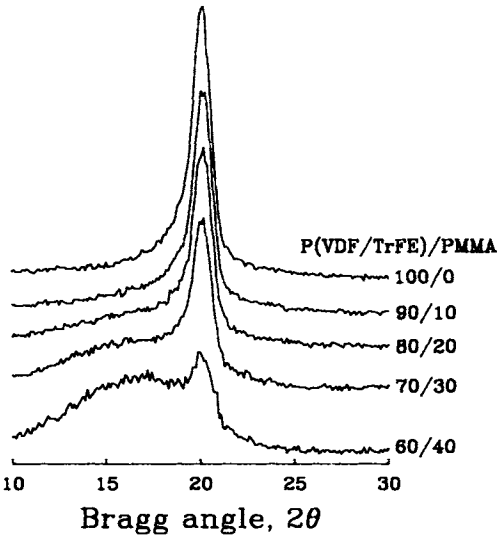

Figure 8 X-ray diffractograms of the P(VDF/TrFE)/PMMA blends with various compositions.

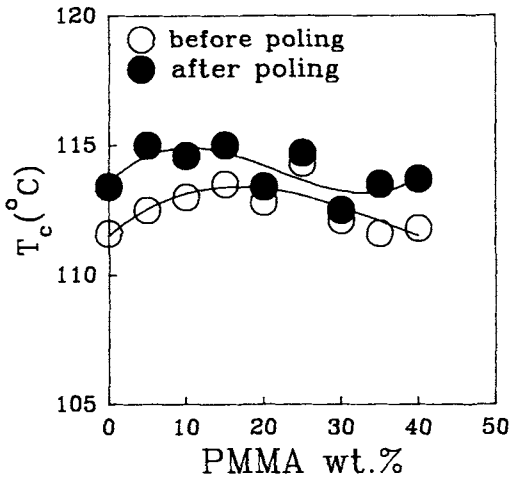

Figure 9 Plots of the Curie transition temperature as a function of the PMMA content before and after poling.

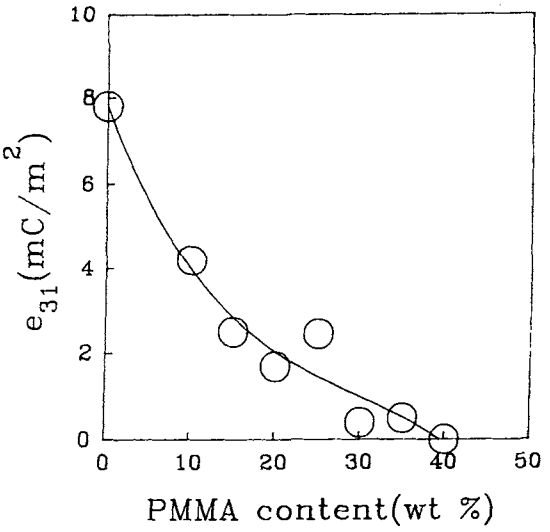

Figure 11 Plots of the piezoelectric stress constant as a function of the PMMA content.

responding to the paraelectric peak and the FWHM of the ferroelectric diffraction peak at $2\theta = 20°$ will be diminished. Figure 9 shows the dependence of the Curie transition point on poling with respect to the PMMA content. As expected, the Curie point is increased by 2 or 3°C after poling regardless of the PMMA content and the diminution of the diffraction intensity at $2\theta = 18°$ associated with a paraelectric or amorphous phase is observed for P(VDF/TrFE), as shown in Figure 10. Changes, however, in the blends cannot be observed clearly due to the reduction of crystallinity and the intrinsically low S/N ratio in X-ray diffraction of polymers.

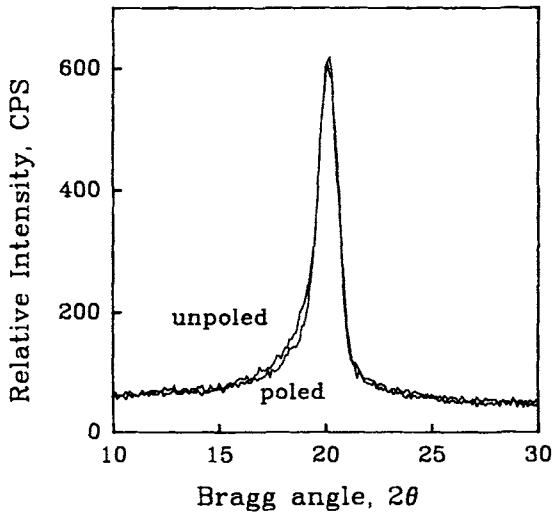

Figure 10 X-ray diffractograms of P(VDF/TrFE) before and after poling.

The influence of PMMA on the piezoelectricity of the blend is shown in Figure 11, where the piezoelectric stress constant e_{31} is plotted as a function of the PMMA content. The e_{31} value drops sharply with an increase of the PMMA content and disappears almost completely as the weight percent exceeds 40. Similar behavior is observed in the A_{884}/A_{848} values of the poled samples shown in Figure 7, which means that the piezoelectric properties are highly related to the degree of irreversible alignment of the CF dipoles in the ferroelectric crystal phase during poling. Therefore, the rapid reduction of piezoelectricity is associated mainly with a rapid decrease of ferroelectric crystallinity due to the dilution with PMMA.

CONCLUSION

Slower cooling rates from the melt during paraelectric crystallization lowers T_c, increases the portion of F_β at the expense of the F_α portion, and produces larger amounts of the unstable ferroelectric phase. $T_c^{\downarrow}$ is rarely dependent upon the amount of PMMA, but $T_c^{\uparrow}$ increases with the PMMA content. PMMA induces the long-*trans* isomer defects in the paraelectric phase, larger portions of F_α after $P \Rightarrow F$ transition, and small *gauche* defects in the ferroelectric phase, i.e., which can easily be stabilized to the ferroelectric crystal during reheating. PMMA also lowers the degree of crystallinity. The increasing content of PMMA reduces electric response and piezoelectricity drastically due to the lower degree of

ferroelectric crystallinity. The ferroelectric crystal phase becomes more stable and *gauche* defects are reduced through structural reorganization during poling.

This work was supported by the Korea Science and Engineering Foundation (KOSEF) under grant KOSEF 901-1005-01201.

REFERENCES

1. T. Furukawa, M. Date, E. Fukuda, Y. Tajitsu, and A. Chiba, *Jpn. J. Appl. Phys.*, **19,** L109 (1980).
2. K. Tashiro, K. Takano, M. Kobayashi, Y. Chatani, and H. Tadokoro, *Ferroelectrics,* **57,** 297 (1984).
3. K. Tashiro, K. Takano, M. Kobayashi, Y. Chatani, and H. Tadokoro, *Polymer,* **25,** 195 (1984).
4. J. S. Green, B. L. Farmer, and J. F. Rabolt, *J. Appl. Phys.*, **60,** 2690 (1986).
5. K. J. Kim, N. M. Reynolds, and S. L. Hsu, *Macromolecules,* **22,** 4395 (1989).
6. A. J. Lovinger, T. Furukawa, G. T. Davis, and M. G. Broadhurst, *Polymer,* **24,** 1225 (1983).
7. G. T. Davis, T. Furukawa, A. J. Lovinger, and M. G. Broadhurst, *Macromolecules,* **15,** 329 (1982).
8. M. V. Fernandez, A. Suzuki, and A. Chiba, *Macromolecules,* **20,** 1806 (1987).
9. T. Yagi, M. Tatamono, and J. Sako, *Polym. J.*, **12,** 209 (1980).
10. T. Yamada, T. Ueda, and T. Kitayama, *J. Appl. Phys.*, **52,** 948 (1981).
11. G. M. Stack and R. Y. Ting, *J. Polym. Sci. Polym. Phys. Ed.*, **26,** 55 (1988).
12. T. Furukawa and G. E. Johnson, *J. Appl. Phys.*, **52,** 940 (1981).
13. N. Koizumi, Y. Murata, and Y. Oka, *Jpn. J. Appl. Phys.*, **23,** L324 (1984).
14. N. Koizumi, N. Haikawa, and H. Habuka, *Ferroelectrics,* **57,** 99 (1984).
15. G. A. Samara, *J. Polym. Sci. Polym. Phys. Ed.*, **27,** 39 (1989).
16. K. Tashiro, S. Nishimura, and M. Kobayashi, *Macromolecules,* **21,** 2463 (1988).
17. H. Tanaka, H. Yukawa, and T. Nishi, *Macromolecules,* **21,** 2469 (1988).
18. G. T. Davis, M. G. Broadhurst, A. J. Lovinger, and T. Furukawa, *Ferroelectrics,* **57,** 73 (1984).
19. K. Koga and H. Ohigashi, *J. Appl. Phys.*, **59,** 2142 (1986).
20. K. J. Kim, G. B. Kim, and S. H. Han, in *2nd Pacific Polymer Conference,* Otsu, Japan, Nov. 26–29, 1991, p. 501.
21. P. R. Sundarajan and P. J. Flory, *J. Am. Chem. Soc.*, **96,** 5025 (1974).
22. K. Saito, S. Miyata, T. T. Wang, Y. S. Jo, and R. Chujo, *Macromolecules,* **19,** 2450 (1986).
23. N. M. Reynolds, K. J. Kim, C. Chang, and S. L. Hsu, *Macromolecules,* **22,** 1092 (1989).
24. G. T. Davis, M. G. Broadhurst, A. J. Lovinger, and T. Furukawa, *Ferroelectrics,* **57,** 73 (1984).
25. Y. Tajitsu, H. Ogura, A. Chiba, and T. Furukawa, *Jpn. J. Appl. Phys.*, **26,** 554 (1987).
26. K. J. Kim, N. M. Reynolds, and S. L. Hsu, *Macromolecules,* to appear.

Received April 15, 1992
Accepted May 27, 1992